Biomaterials 271 (2021) 120740

Contents lists available at ScienceDirect

Biomaterials

journal homepage: www.elsevier.com/locate/biomaterials

Discovery of synergistic material-topography combinations to achieve immunomodulatory osteoinductive biomaterials using a novel in vitro screening method: The ChemoTopoChip

Laurence Burroughs [a], Mahetab H. Amer [a], Matthew Vassey [a], Britta Koch [a], Grazziela P. Figueredo [a], Blessing Mukonoweshuro [a], Paulius Mikulskis [a], Aliaksei Vasilevich [b], Steven Vermeulen [c], Ian L. Dryden [a], David A. Winkler [a,d,e,f], Amir M. Ghaemmaghami [a], Felicity R.A.J. Rose [a], Jan de Boer [b,1], Morgan R. Alexander [a,*,1]

[a] University of Nottingham, Nottingham, NG7 2RD, United Kingdom
[b] Eindhoven University of Technology, Eindhoven, 5600 MB, Netherlands
[c] MERLN Institute for Technology-inspired Regenerative Medicine, Maastricht, 6229 ER, Netherlands
[d] Medicinal Chemistry, Monash Institute of Pharmaceutical Sciences, Parkville, 3052, Australia
[e] La Trobe Institute for Molecular Science, La Trobe University, Bundoora, 3042, Australia
[f] CSIRO Data61, Clayton, 3168, Australia

ARTICLE INFO

Keywords:
Biomaterials
Mesenchymal stem cells
Macrophages
Regenerative medicine

ABSTRACT

Human mesenchymal stem cells (hMSCs) are widely represented in regenerative medicine clinical strategies due to their compatibility with autologous implantation. Effective bone regeneration involves crosstalk between macrophages and hMSCs, with macrophages playing a key role in the recruitment and differentiation of hMSCs. However, engineered biomaterials able to simultaneously direct hMSC fate and modulate macrophage phenotype have not yet been identified. A novel combinatorial chemistry-topography screening platform, the ChemoTopoChip, is used here to identify materials suitable for bone regeneration by screening 1008 combinations in each experiment for human immortalized mesenchymal stem cell (hiMSCs) and human macrophage response. The osteoinduction achieved in hiMSCs cultured on the "hit" materials in basal media is comparable to that seen when cells are cultured in osteogenic media, illustrating that these materials offer a materials-induced alternative to osteo-inductive supplements in bone-regeneration. Some of these same chemistry-microtopography combinations also exhibit immunomodulatory stimuli, polarizing macrophages towards a pro-healing phenotype. Maximum control of cell response is achieved when both chemistry and topography are recruited to instruct the required cell phenotype, combining synergistically. The large combinatorial library allows us for the first time to probe the relative cell-instructive roles of microtopography and material chemistry which we find to provide similar ranges of cell modulation for both cues. Machine learning is used to generate structure-activity relationships that identify key chemical and topographical features enhancing the response of both cell types, providing a basis for a better understanding of cell response to micro topographically patterned polymers.

1. Introduction

Bone repair is a complex and highly organized process involving interactions between multiple cell types, molecular signals, and interactions with the extracellular environment [1]. Currently, autologous bone grafts remain the gold standard in bone regeneration because of their osteogenicity, osteoinductivity, osteoconduction and osteointegration characteristics [2,3]. Synthetic bone substitutes, such as calcium phosphate (CaP) ceramics, have proven safe and biocompatible but often lack the osteogenicity needed to support bone healing [4]. There is great interest in the use of hMSCs in combination with synthetic biomaterials to provide a potential way of overcoming these challenges in

* Corresponding author.
E-mail address: morgan.alexander@nottingham.ac.uk (M.R. Alexander).
[1] Joint Senior Authors.

https://doi.org/10.1016/j.biomaterials.2021.120740
Received 29 September 2020; Received in revised form 26 January 2021; Accepted 25 February 2021
Available online 1 March 2021

autologous bone grafting [5,6].

The inherent multipotency of hMSCs has allowed in vitro culture models to be used, in combination with synthetic biomaterials, to differentiate cells into osteoblasts without osteogenic supplements [7]. MSCs have also been shown to form bone *in vivo* driven by nano topography [5], protein adsorption to surface chemistry [6] and phosphorus delivery to the cells [8,9]. Furthermore, there is growing evidence demonstrating a reciprocal functional role of macrophage polarization in hMSC osteoblast differentiation, with pro-healing M2 macrophages having previously been reported to enhance hMSC osteoblastic differentiation [10]. The crosstalk between macrophages and MSCs is considered to play a key role in normal bone repair [11–13].

Combinatorial screening has been used by the materials community for over 20 years as a tool for identification of biomaterials when the underlying theory required for rational design is undeveloped [14]. Microarrays of polymer spots have successfully identified new materials by determining cell response against large and diverse polymer libraries to identify novel materials supporting pluripotent human embryonic stem cell expansion [15,16], and differentiation into cardiomyocytes [17] and hepatocytes [18]. Polymers capable of inducing macrophage polarization [19] or resisting bacterial attachment [20] have also been identified using a similar approach, with devices coated in bacterial resistant polymers recently progressing to clinical trials [21].

Topographical patterning of surfaces has been shown to direct cell attachment at the microscopic scale [22]. At the nanoscale, phenotypic control has been demonstrated and rationalized in terms of adsorbed protein and effects on cell contractility of focal adhesion formation [5,6,23]. Simple geometric shapes such as grooves/ridges, pillars and pits have been investigated [24,25]; to screen complex microtopographies derived combinatorially, a high-throughput microtopography screening platform, the TopoChip, was developed [26]. This used mathematical algorithms capable of designing millions of possible topographical features from circle, triangle and rectangle primitives (sized 3–23 μm laterally and 10 μm vertically). A subset of these was arranged periodically to form 290 × 290 μm Topo units, which are analogous to the polymer spots in combinatorial chemistry microarrays. A total of 2176 Topo units were fabricated on each 2 × 2 cm TopoChip using UV photolithography to form a master from which polymers could be embossed with the topographies for cell screening. This allowed a much wider selection of topographies to be screened than previously, freed the process from the constraints of simple geometric form, and used machine-learning to predict new structures likely to elicit desirable cell responses [26–29].

The ability to tune or modulate the foreign-body response to a biomaterial is an ongoing challenge in the field of regenerative medicine [30–32]. This is further complicated when designing materials for tasks such as induction of osteogenic differentiation of hMSCs at the site of implantation. Surface chemistry [15,16,33] and surface topography [27,34–36] have both been shown to enhance the differentiation and proliferation of stem cells yet, to our knowledge, biomaterials have not been reported capable of simultaneously directing differentiation of hMSCs and polarizing macrophages towards an M2 state. In order to allow the role of both material chemistry and topography to be surveyed in the field of material-driven bone-regeneration a combinatorial high-throughput screening tool, the *ChemoTopoChip,* was developed in this work.

2. Materials and Methods

2.1. Methacrylate functionalization of glass slides

Glass slides (26 mm × 50 mm × 0.40 mm) are activated using O_2 plasma ($p_i = 0.3$ mbar, 100 W, 1 min) and immediately transferred into dry (4 Å MS) toluene (50 mL) under argon. 3-(Trimethoxysilyl) propyl methacrylate (1 mL) is added, and the reaction mixture heated to 50 °C for 24 h. The slides are then cooled to room temperature and washed by sonication with 3 × 10 mL fresh toluene. The slides are then dried under vacuum in a silicone-free vacuum oven (50 °C) for 24 h.

2.2. Molding of TMPMP-co-TEGDA substrate

TEGDA (337 μL) and TMPMP (163 μL) are added together under argon with DMPA (16.9 mg). The mixture is then sonicated for 15 min to ensure mixing. Each ChemoTopoChip mold on the silicon wafer is framed on 3 sides with Scotch tape (3 M) spacers, and a methacrylate silanized glass slide placed on top of each ChemoTopoChip to be molded; standard glass microscope slides (25 mm × 75 mm × 1.0 mm) are placed on top as weights to hold the silanized slides in place. The TMPMP/TEGDA reaction mixture is transferred into an argon glove box (<2000 ppm O_2) along with the silicon mold, and the monomer solution (60 μL) pipetted between the silicon wafer and silanized slides. The rate of pipetting was manually maintained at a similar rate to that of the capillary forces acting upon the solution. When all ChemoTopoChip positions have been pipetted (~10 min per ChemoTopoChip) they are irradiated with UV light (368 nm, 2 × 15 W bulbs, 10 cm from source) for 10 min. Once complete, the entire molding setup is removed from the glove box and the glass microscope slide weights removed. The silicon wafer is then placed on to a pre-heated (70 °C) hot plate; after 10 min, the molded ChemoTopoChips are carefully removed using a scalpel (CAUTION: excessive force and speed will break the thin glass substrate). Once removed, the molded ChemoTopoChips are cleaned by sonication in acetone (10 mL, 10 min) then isopropyl alcohol (10 mL, 10 min). Finally, the ChemoTopoChips are dried under vacuum (0.3 mbar) for 24 h before functionalization.

2.3. Functionalization of molded ChemoTopoChip samples

Monomer solutions are made up as follows: 75% v/v in *N*,*N*-dimethylformamide (DMF) for oils; 50% w/v in DMF for solids. Next, 0.05% w/v photoinitiator DMPA is added to these solutions before degassing by sonication (10 min). The molded ChemoTopoChip samples are then transferred into an argon glove box (<2000 ppm O_2) along with these monomer solutions. A total of 3 μL of monomer solution is then applied to each respective ChemoTopo unit, taking care to evenly cover the entire area required for functionalization. The ChemoTopoChips are then irradiated with UV light (368 nm, 2 × 15 W bulbs, 10 cm from source) for 15 min during which reaction with the surface thiols and polymerization of the monomer occurs, before being removed from the argon glove box and sonicated in isopropanol for 10 min. Due to the lower bond dissociation energy of the acrylate π-bond [37] compared with that of the thiol σ-bond [38], it is expected that these monomers will polymerize to the thiol moieties on the base TMPMP-co-TEGDA substrate after photoinitiation commences. The samples are then placed under vacuum (0.3 mbar) for 7 days before use.

2.4. Time-of-flight secondary-ion mass spectrometry (ToF-SIMS) analysis

ToF-SIMS analysis was carried out using a ToF-SIMS IV (IONTOF GmbH) instrument operated using a 25 kV Bi_3^+ primary ion source exhibiting a pulsed target current of ~1 pA. Samples were scanned at a pixel density of 100 pixels per mm, with 8 shots per pixel over a given area. An ion dose of 2.45×10^{11} ions per cm^2 was applied to each sample area ensuring static conditions were maintained throughout. Both positive and negative secondary ion spectra were collected. Owing to the non-conductive nature of the samples, a low energy (20 eV) electron flood gun was applied to provide charge compensation.

2.5. Atomic force microscopy (AFM) analysis

AFM measurements were conducted using a Bruker Dimension FastScan Bio Icon AFM in Peak Force™ (Tapping) mode. Scan areas were 500 × 500 nm and 4 regions of interest (ROIs) were taken. Bruker

RTESPA-150 probes were used for all analyses, with all results calibrated to a Bruker polystyrene (2.7 GPa) standard.

2.6. X-ray photoelectron spectroscopy (XPS) analysis

XPS characterization was carried out using a Kratos AXIS ULTRA. Data was processed using CasaXPS version 2.3.20 rev1.2G. Estimation of the functionalized surface layer thickness of the iBOMAm region was carried out using the method described by Ray and Shard as follows [39].

$$d_{N(1s)} = -L_{N(1s)}\, cos\theta\, ln\left(1 - \frac{[N] - [N]_0}{[N]_\infty - [N]_0}\right) \quad \text{(Eq 1)}$$

$$L = 0.00837\, E^{0.842} \quad \text{(Eq 2)}$$

Where $L_{N(1s)}$ is the average polymer electron attenuation length (3.01 nm) calculated from the electron kinetic energy of the N1s electrons E (1085.5 eV), θ is the electron take-off angle (0°), $[N]$ is the nitrogen atomic fraction in the measured sample layer (1.08%), $[N]_0$ is the nitrogen atomic fraction in the pure substrate layer (0%), $[N]_\infty$ is the nitrogen atomic fraction in the pure sample layer (9.10%).

2.7. Mesenchymal stem cell culture

Human immortalized mesenchymal stem cells (hiMSCs) were generated in-house by lentiviral transfection of E6/E7 and hTERT genes as previously described [40,41]. Cells were cultured in Dulbecco's modified Eagle's medium supplemented with 10% (v/v) foetal bovine serum, 1% (v/v) penicillin-streptomycin and 1% L-glutamine (Basal media). Positive controls were cultured in Human Mesenchymal Stem Cell (hMSC) Osteogenic Differentiation Medium (PT-3002; Lonza), which is supplemented with dexamethasone, L-glutamine, ascorbate, penicillin/streptomycin and β-glycerophosphate. All cells were maintained in a humidified incubator at 37 °C and 5% CO_2 in air. Cells were re-suspended in the appropriate volume of media and seeded on 3 replicate ChemoTopoChips at 1×10^5 hiMSCs/chip (3 independent experiments using cells from 3 different passage numbers).

2.8. hiMSC immunofluorescence staining

For alkaline phosphatase (ALP) staining, cells were cultured on the ChemoTopoChips for five days in culture medium (at 37 °C, 5% CO_2 in air), then fixed using 70% (v/v) ethanol, permeabilized with 0.1% (v/v) Triton X-100 and incubated with a blocking solution of 3% (v/v) goat serum in 1% (v/v) BSA/PBS. Staining was carried out using human ALP antibody (Dilution 1:50; sc137213, Santa Cruz Biotech) and counterstained for α-tubulin (2 μg/mL; PA120988, Invitrogen) for 3 h at room temperature. After washing, slides were incubated with the appropriate secondary antibodies in the green and red channels at room temperature (1:100 dilution). Nuclei were stained with NucBlue Fixed Cell ReadyProbes™ (Invitrogen).

2.9. Monocyte isolation and culture

Buffy coats were obtained from the National Blood Service after obtaining written informed consent and approval from the ethics committee. Monocytes were isolated from peripheral blood mononuclear cells (PBMCs). A MACS magnetic cell separation system (CD14 MicroBeads positive selection with LS columns, Miltenyi Biotec) was used for the isolation as previously described [19,42]. Isolated monocytes (>95% purity) were suspended in RPMI-1640 medium containing 10% foetal bovine serum (FBS), 100 μg/ml streptomycin, 2 mM L-glutamine and 100 U/ml penicillin (Sigma-Aldrich). For assessment of cell attachment and phenotype characterization, cells were re-suspended in the appropriate volume of media and seeded on the ChemoTopoChips at 2×10^6 monocytes/chip and incubated at 37 °C, 5% CO_2 in a humidified incubator for 9 days.

2.10. Macrophage immunofluorescent staining

On day 9 all adherent cells cultured on ChemoTopoChips were fixed in 4% paraformaldehyde (BioRad) in PBS, then blocked with 3% BSA (Sigma-Aldrich) and 1% Glycine (Fisher Scientific) in PBS. Subsequently, another blocking step was carried out using 5% goat serum (Sigma) in PBS. Adherent cells were stained with 2 μg/mL anti-human TNFα (IgG1) mAb (Abcam), and with 1 μg/ml anti-human IL-10 (IgG1) mAb (Abcam) followed by 1 h incubation at room temperature. After washing, cells were stained with 8 μg/ml Rhodamine-x goat anti-mouse IgG (H + L) secondary Ab (Invitrogen), and 8 μg/ml Alexa flour-647 goat anti-rabbit IgG (H + L) secondary antibody (Invitrogen) for another hour at room temperature. All samples were counterstained with 250 ng/ml DAPI (4′,6-Diamidino-2-Phenylindole) (Invitrogen) at room temperature.

2.11. ChemoTopoChip imaging

Imaging of all fixed and stained ChemoTopoChip samples was carried out using a widefield deconvolution-TIRF3 system (Zeiss, custom setup). Imaging was carried out in wide field mode using a 20 × /0.5 NA air objective in the bright field and fluorescence channels with the excitation at 358 nm, 488 nm and 561 nm. The software used to capture was Zeiss Zen Blue, by using the "Sample Carrier Designer" wizard/module to manually create and calibrate the position list which was used to scan all the positions in the chip setup.

2.12. CellProfiler analysis

A custom CellProfiler [43] pipeline was created to correct for uneven background illumination in each image, then each image cropped to within the Topo unit 30 μm wall. Nuclei were detected using an adaptive per-object algorithm in the blue channel images, followed by propagation from these primary detected objects to detect cell cytoskeleton and ALP staining (hiMSCs) or TNFα and IL-10 (human macrophages) in the green and red channel images. Intensity of detected objects was measured and exported, and images containing overlaid outlines of detected objects also saved to ensure correct operation of the pipeline.

2.13. Statistical analysis

Statistical analysis and graphical plots were carried out in R version 3.6.1 using RStudio version 1.2.1335 as integrated development environment (IDE). For an exploratory method, combinations having p-value < 0.05 were highlighted from a two independent sample equal variance *t*-test; the Benjamini and Hochberg false discovery rate method was used to adjust the p-values to minimise type I errors due to multiple comparisons [44]. The values were normalized to the base polymer region on each slide. Heatmaps were plotted using the heatmap.2 function from the gplots package version 3.1.0.2 in combination with the RColorBrewer package version 1.1–2. Clustering and dendrograms for heatmaps were produced using the complete linkage method [45] with Euclidean distance measure. Ranked scatter plots and box plots were carried out using base functions in R and the ggplot2 package version 3.2.1.

2.14. Synergy ratio determination

Assessment of the interactions between binary factors (chemistry and topography) is readily performed using a synergy ratio (*SR*). Taking the cell response (e.g. attachment or phenotype) to factor x_1 alone (y_1), the response to factor x_2 alone (y_2) and the response to the factors combined x_{12} (y_{12}), *SR* can be calculated as shown in Equation Eq (3):

$$SR = \frac{y_{12}}{y_1 + y_2} \quad \text{(Eq 3)}$$

For a synergistic combination, $SR > 1$ as the ratio is then greater than the sum of the theoretical maximums of the individual response factor comparators; for a counteractive combination, SR < 0.5 as the ratio is then less than the theoretical maximum of one individual response factor alone (i.e. 0 contribution from the second individual response factor). In analysis of the ChemoTopoChip data, unfunctionalized TMPMP-co-TEGDA molded topographies and flat area chemistries were used as the individual factors x_1 and x_2 to compare with the hit topography-material combinations x_{12}.

4.15. Random forest machine learning

The raw dataset consisted of three technical repeats for each surface variable (topography, chemistry) within a chip, which were further replicated across multiple batches (biological repeats). Data set from repeats in a chip have been normalized against their correspondent flat values. Subsequently, replicate average values were calculated. The average between batches was then determined as the dependent variable for the predictive models. Macrophage polarization and ALP intensity predictive models were generated.

The various topographies were encoded using descriptors generated by CellProfiler [43] that relate directly to particular primitives in the topographical units. For chemistries, 1-hot descriptors (binary variables indicating the presence or absence of a chemistry in any given combination) were used.

The SHapley Additive exPlanation (SHAP) method was used for feature selection to eliminate uninformative and less informative descriptors and less relevant chemistries. SHAP was implemented using the SHAP package in Python 3.7. Regression models were generated using the random forest approach with the scikit-learn package in Python 3.7. The default parameters from version 0.22 were adopted for the random forest models. That is, 100 estimators were considered using gini as the function to measure the quality of the data instances split. And no limit for the maximum depth of the trees was defined. 70% of the data instances were employed for model training and 30% for testing using Bootstrapping without replacement; we ran the model 50 times with different training/test sets randomly selected and calculated the average and standard deviation of those runs.

3. Results and discussion

The ChemoTopoChip layout is presented in Fig. 1(a–c) with the chemistries and the topounit designs presented in Fig. 2. This platform contains 1008 microtopography and materials chemistry combinations to simultaneously probe their combined effects on cellular response. This is effectively a combination of the polymer microarray approach and the TopoChip platforms to facilitate identification of synergistic chemistry-topography combinations, and elucidation of structure-function relationships between cells and material cues.

The design comprised 36 Topo units of size 500 × 500 μm, including one flat control (Fig. 1b) arranged in 3 × 3 mm sized ChemoTopo units. These are repeated 28 times, each with a different chemical functionalization. The microtopographies are 10 μm high and were chosen from previous TopoChip screens to maximize the morphological differences of MSCs (Fig. 2) [36]. The chemistries were chosen from libraries of (meth)acrylate and (meth)acylamide monomers to provide maximum chemical diversity (see Fig. 2 for structures and classification of their number of H-bond donors, number of H-bond acceptors and log partition coefficient. The monomers are used to functionalize the surface of topographically molded chips, which minimizes differences in material

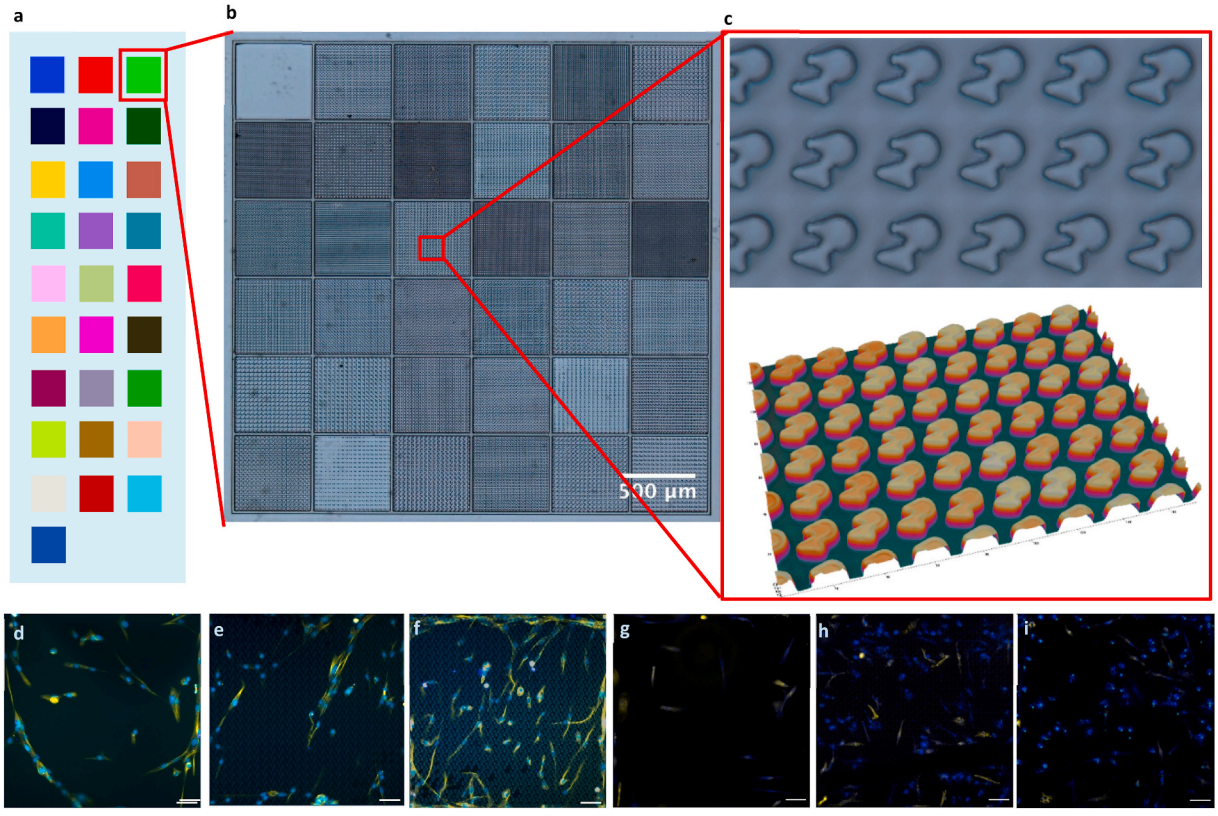

Fig. 1. a) Schematic showing ChemoTopoChip layout with colors representing different chemistries; b) Interference profilometer imaged ChemoTopo unit (30 μm high walls separate each Topo unit); c) Example features from a ChemoTopo unit; hiMSCs (blue = ALP, yellow = α-tubulin); on d) flat TMPMP-co-TEGDA area e) TMPMP-co-TEGDA + Topo 3 area; f) mMAOES + Topo 3 area; Macrophages (blue = IL-10, yellow = TNFα) on g) flat TMPMP-co-TEGDA area; h) TMPMP-co-TEGDA + Topo 22 area; i) BzHPEA + Topo 22 area. (For interpretation of the references to color in this figure legend, the reader is referred to the Web version of this article.)

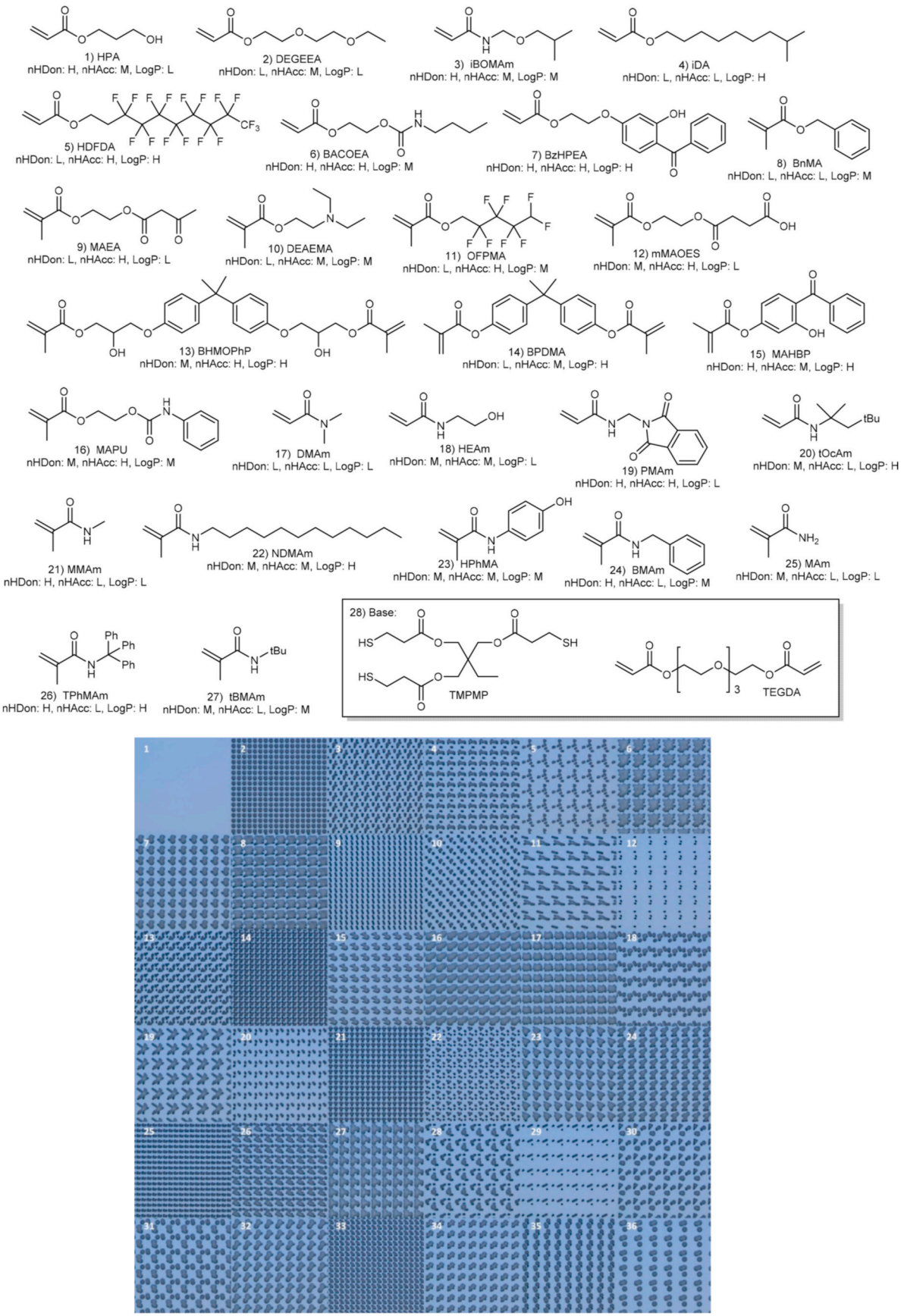

Fig. 2. Chemistries Used in the ChemoTopoChip: nHDon, nHAcc and LogP refer to number of H-bond donors, number of H-bond acceptors and LogP (octanol/water partition coefficient) classified as high (H), medium (M) or low (L) and magnified images of the features and their arrangements in the topounits along with their codes.

compliance between the different chemistries. The modulus measured by AFM was found not to vary greatly, as anticipated for surface modification of the underlying polymer (Table S1).

A silicon mold was fabricated from the ChemoTopoChip design using photolithography and etching to produce the negative master of the topographies. The desired features were produced from this master by injecting a 1:2 mixture of trimethylolpropane tri(3-mercaptopropionate): tetra(ethylene glycol) diacrylate (1:2 TMPMP: TEGDA) monomers containing the photoinitiator 2,2-dimethoxy-2-phenylacetophenone (DMPA) between a methacrylate-functionalized glass slide and the silicon master. UV curing and solvent washing then provided the molded ChemoTopoChip substrate, chosen because similar photopolymerized thiol-ene systems have been reported as tough shape memory, flexible materials offering low shrinkage stress that are sufficiently transparent to allow transmission optical imaging [46]. Functionalization of the ChemoTopo units was carried out by deposition of 50% w/v or 75% v/v monomer solutions in *N*,*N*-dimethylformamide (DMF) containing 0.05% w/v DMPA onto each ChemoTopo unit prior to UV curing and washing. Imaging surface analysis (ToF-SIMS) was used to determine to localization of the chemistries, which were found to be confined to the desired areas in Fig. S1. Elemental and functional composition was determined by XPS and found to be consistent with the expected surface chemical modification for an amide where the nitrogen signal increases, Fig. S2. Estimation of the surface layer thickness using the XPS determined nitrogen composition of the monomer for an acrylamide provided a value of approximately 0.4 nm [39].

3.1. hiMSC differentiation

To identify materials that can direct hiMSC differentiation towards an osteoblastic lineage and that induce human macrophages polarization towards a pro-healing M2 phenotype, we first investigated the osteoinductive potential of the materials. The hiMSC used in the study are well-characterized [40,41] and retain the capacity to differentiate to the osteoblastic lineage. hiMSCs were seeded on 3 replicate chips in 3 independent experiments and cultured in basal culture media. This culture media was not supplemented with any exogenous osteo-inductive factors. Positive and negative controls were included to illustrate the baseline osteogenic potential of these cells on control substrates in comparison to the test surfaces. After 5 days, samples were fixed and stained for both α-tubulin (cytoskeletal marker) and alkaline phosphatase (ALP, an early osteogenic marker), and analyzed using an automated high-throughput fluorescence microscope. Fluorescence α-tubulin images from two representative substrate chemistries are presented in Figs. S3 and S4. ALP expression is a widely used early osteogenesis marker as it is known to be involved in bone formation, plays an essential role in matrix mineralization and is induced by a range of osteogenic molecules [47]. Images were processed using CellProfiler software [43] to quantify cell number and ALP staining intensity on each individual topography-material combination. The ALP staining intensity and attached cell number were both normalized to that of the flat TMPMP-co-TEGDA Topo unit within each ChemoTopoChip sample. Mineralization was not assessed, using von Kossa staining or Alizarin Red for example, as these methods were deemed unsuitable for this screening tool due to their qualitative nature when imaged and lack of compatibility with the high-throughput imaging methodology employed (CellProfiler).

A diverse range of hiMSC morphologies and attached cell numbers were seen across the ChemoTopoChip. The stem cells displayed an elongated shape and on some ChemoTopo units with alignment to the topographies, e.g. as seen in Fig. 1e, in contrast to more uniform cell spreading and random alignment on others and on the flat chemistry as seen in Fig. 1d. The stem cell response to iBOMAm and the base TMPMP-co-TEGDA chemistries are presented in Figs. S3 and S4 to illustrate the variation in cell morphology and alignment. Previous TopoChip screens using hMSCs revealed a similar range of cell morphological responses, where more elongated cells were linked to ALP upregulation [27,36].

To ascertain the magnitude of the ALP upregulation we compared the mean fluorescence intensity per cell of the hiMSC cells differentiated in osteo-inductive media with the response of cells cultured in basal media on the chip (supplements detailed in Materials and Methods). No difference in ALP upregulation was observed between the top 50 ChemoTopoChip ALP hits and the positive control sample cultured in osteogenic media ($p < 0.001$, see Fig. 3). These materials therefore induce a similar osteogenic state of the cells, as measured by ALP upregulation, to that of osteo-inductive supplements commonly used to differentiate hMSCs to osteoblasts. In the absence of stimulatory materials chemistry-topography combinations, the ALP intensity was significantly lower as seen for the lowest 50 combinations.

To interrogate the range and magnitude of the cell effects from this large range of chemo-topo combinations, we found it is useful to plot all the results as clustered heatmaps, which groups the most similar responses of chemistries across all topographies and vice versa (Fig. 4a), and as rank ordered plots to illustrate the range of cell response for all ChemoTopo units (Fig. 4c). Alternative versions of the heatmap without clustering are shown in Fig. S10 to facilitate individual combination comparisons. To focus the data interrogation, we indicate the combinations which were determined to have p-value < 0.05 from a two independent sample equal variance *t*-test, with p-values adjusted using the Benjamini and Hochberg method [44] to minimise type I errors due to the large number of different substrates compared. Analysis of the mean integrated ALP expression per cell for each topography-material combination showed that 3 exhibited significant upregulation of this osteogenic marker ($p < 0.05$) compared to the flat base Topo unit (see Table S2 for full list), with all of these displaying a higher ALP intensity than the flat base material region used as a control comparator. Visual inspection of the heatmaps and ranked scatter plots reveals trends across various chemistries, e.g. monomers 12 (mono-2-(methacryloyloxy)ethyl succinate, mMAOES) and 20 (*N*-tert-octylacrylamide, tOcAm), suggesting that a group of chemistries induce upregulation of ALP intensity relative to the mean; equivalent topographical trends were less evident indicating that topographical stimuli did not dominate across the range of chemistries used (see Fig. 4a and c). A total of 103 combinations were found to have higher normalized cell number than the flat base region used as the control ($p < 0.05$, total area taken into account), but none lower (Table S2 for full list). All combinations containing topographies showed greater cell numbers than those of chemistries on flat surfaces (Topo 1), suggesting that topography was also a driver for hiMSC attachment (see Figs. S5 and S6a). Future studies will benefit from the methodologies identified herein which to investigate these synergistic combinations on scaled up samples which will allow further markers of osteoblastic differentiation and to study donor variability using primary bone marrow derived mesenchymal stem cells.

3.2. Macrophage polarization

The immunomodulation effect of material-topography combinations was screened by seeding primary human monocytes onto ChemoTopoChips for 6 days followed by cell counting and immunohistochemical fluorescent readouts to estimate differentiation into macrophages and polarization to the M1 or M2 phenotype. Monocytes were isolated from peripheral blood of two independent donors, with 3 replicates carried out for each. Compared to surface phenotype, cytokine profile of macrophages is a more accurate indicator of their functional phenotype with tumor necrosis factor α (TNF-α) and interleukin-10 (IL-10) as archetypal pro- and anti-inflammatory cytokines respectively. Thus, to determine the polarization status of the cells, samples were fixed and stained for intracellular expression of TNFα (M1 polarization indicator) and IL-10 (M2 polarization indicator) respectively, and analyzed using high-throughput fluorescence microscopy. Images were processed using CellProfiler software [43] with an image analysis pipeline designed to quantify cell attachment using DAPI nuclear

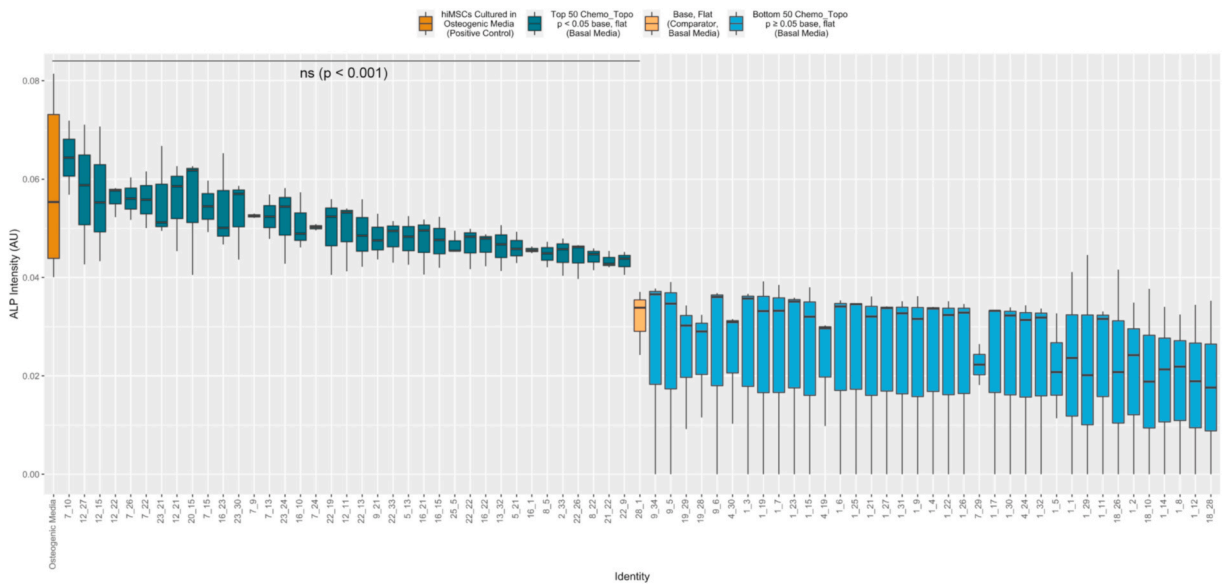

Fig. 3. Raw ALP Intensities of hiMSCs cultured on the top 50 ChemoTopo combinations ($p < 0.05$) and bottom 50 ChemoTopo combinations ($p \geq 0.05$) compared to flat base TPMP-co-TEGDA region in basal media, and hiMSCS cultured in osteogenic media.

staining and quantification of the mean fluorescence intensity (MFI) across each Topo unit for the IL-10 and TNFα channels. The IL-10 and TNFα MFI and cell number were normalized to the values from the flat base TMPMP-co-TEGDA Topo unit. The ratio of M2/M1 cells was taken to be the ratio of the IL-10/TNFα MFIs.

Plotting the normalized macrophage cell number and M2/M1 ratio as a scatter plot rank ordered by topography (Fig. 4d) and as clustered heatmaps (Fig. 4b; alternative versions of the heatmap without clustering are shown in Fig. S10 to facilitate individual combination comparisons) indicated that chemistry may have a greater influence over human macrophage polarization than topography. This is in large part due to the significant influence of the M2/M1 ratio provided by material chemistries: 2-(4-benzoyl-3-hydroxyphenoxy)ethyl acrylate (BzHPEA), *N*,*N*′-dimethylacrylamide (DMAm) and heptadecafluorodecyl acrylate (HDFDA). These chemistries showed high M2 polarization across a majority of topographies in the ranked scatter plots (Fig. 4d). Horizontal trends across these chemistries could be seen in the heatmap (Fig. 4b), with vertical trends across topographies less apparent. Similar ranges of responses were observed for all topography-material combinations, including those containing flat areas. As was seen with hiMSC attachment, the range of normalized cell number for combinations containing topographies was greater than those for flat areas (see Figs. S7 and S6c); topography is therefore also found to be important for macrophage attachment. Visual inspection identified some topography-material combinations that were hits for both stem cell differentiation and polarizing macrophages to anti-inflammatory phenotype, with BzHPEA (chemistry 7) in combination with topography 22 appearing strongest for both ALP upregulation in hiMSCs and M2 polarization in macrophages (Fig. 4a–d).

To assess the influence of topography and chemistry, flat chemistries and unfunctionalized TMPMP-co-TEGDA molded topographies were used as comparators. Hit topography-material combinations were compared to these controls to assess their synergy ratios (*SR*). For the hiMSC data set, 15 of the 103 hit combinations that showed greater cell numbers than the flat TPMP-co-TEGDA control were determined to be synergistic (Fig. 5a); additionally, 2 of the 3 hit combinations directing osteogenic differentiation were determined to be synergistic (Fig. 5b). For the hiMSC cell number, 2 combinations appeared to be antagonistic (Fig. 5a). For the human macrophage cell number, 2 topography-material combinations exhibited a synergistic effect (Fig. 5c). Of the top 19 human macrophage polarization combinations, 4 were determined to be synergistic (Fig. 5d). A total of 3 combinations were found to promote upregulation of ALP in hiMSCs *and* polarize human macrophages towards an M2 phenotype (Fig. 5b, d-f). The list of best performing polymers (Fig. 5e), include functional groups that will be ionised at physiological pH to display positive (amine), negative (carboxylic acid) and uncharged (hydroxyl), suggesting that surface charge is not a dominant factor in either hiMSC ALP upregulation or macrophage polarization. Visual inspection of the synergistic topographies (Fig. 5f) did not indicate any obvious correlation between the patterns. The top material, BzHPEA in combination with Topo 22, was found to be synergistic for both datasets (Fig. 5b, d).

3.3. Design rules

To extract rules from ChemoTopoChip screening data to inform future materials design, we used machine learning (ML) methods to generate quantitative structure-activity relationships. The data sets used to train the machine learning models consisted of 1008 rows of identifiers for each topography-chemistry pair and columns for the 28 chemistry identifiers and 65 topographical shape descriptors. The final column to the right of the 93 indicator/descriptor columns contained the biological data that is the dependent variable we are seeking to predict. The 1-hot descriptor approach is commonly used in modelling studies to indicate the presence or absence of a feature; in this case the presence of a particular chemistry is denoted by a '1' in the appropriate cell, with all other cells containing '0'. This allows the feature selection algorithms and machine learning models to identify those chemistries and topography descriptors that have the largest impact on biological responses in the cells in the final column. Using this approach, the macrophage and MSC data sets were modelled using the Random Forest machine learning algorithm [48] (Fig. 6).

The performance of the predictive models, and the topographical descriptors that contributed most strongly to the attachment and polarization, are shown in Fig. 6. The figure presents the results of the regression models as well as the features selected. The features are ordered from top to bottom in the order of their average impact on the model output magnitude.

The macrophage M2/M1 ratio model had a strong correlation between the ML-predicted and observed values ($R^2 = 0.73 \pm 0.05$, Fig. 6b). The size of the topographical features was identified as being important for macrophage polarization. Features with mean areas $<50\ \mu m^2$ and

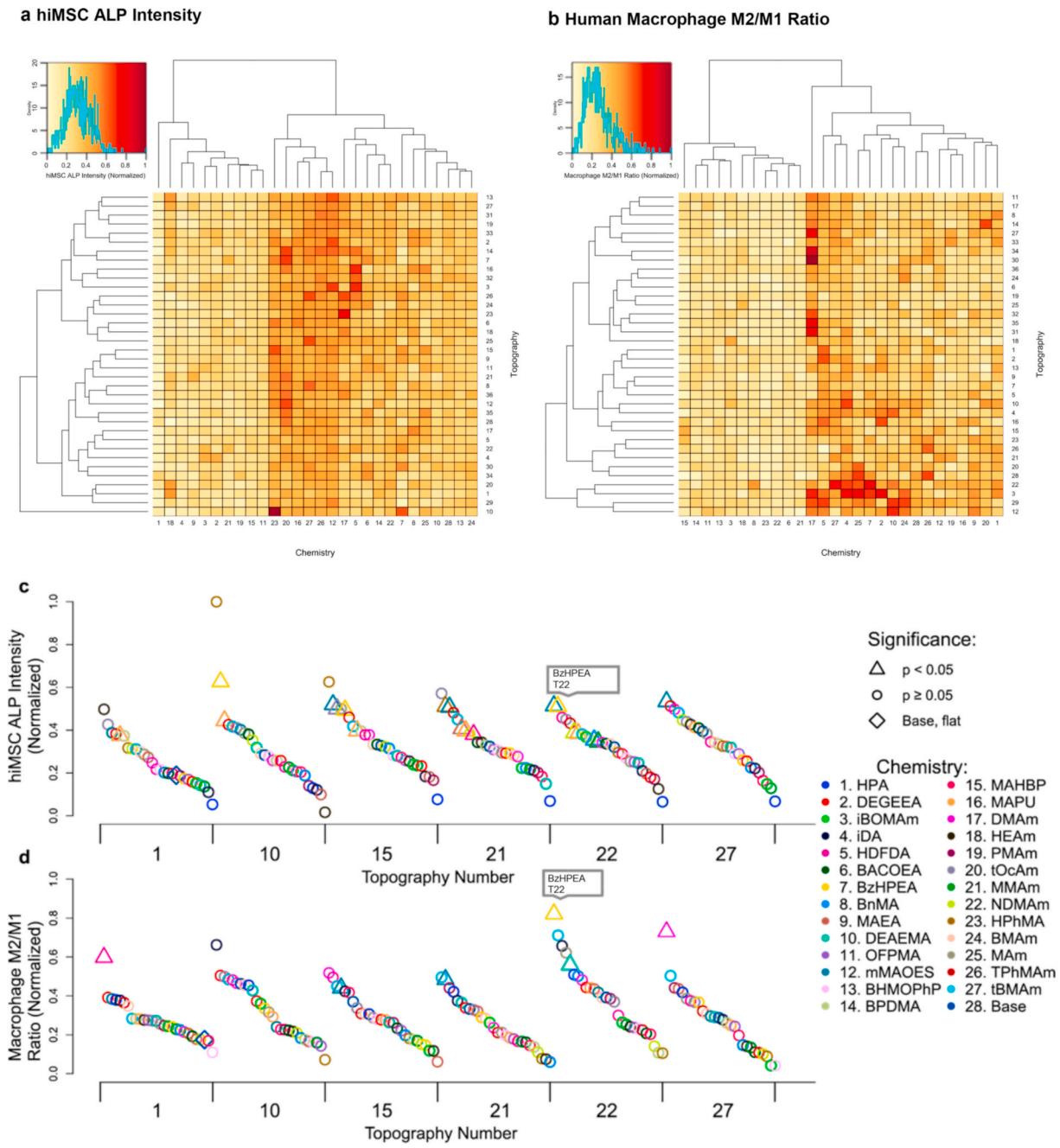

Fig. 4. Clustered heatmaps showing a) Mean integrated hiMSC ALP expression and b) Macrophage M2/M1 ratio across ChemoTopoChip; Rank ordered scatter plots of selected example topographies across all chemistries, showing c) Rank hiMSC ALP intensities across the ChemoTopoChip (N = 3, n = 3, see Figure S6b for full ranked plot) and d) Rank macrophage M2/M1 ratio across the ChemoTopoChip (N = 2, n = 3, see Figure S6d for full ranked plot). In both scatter plots, t-tests are carried out comparing each data point with the base, flat region and statistical significance is donated by triangular symbols ($p < 0.05$); chemistry is donated by color of plot point. (For interpretation of the references to color in this figure legend, the reader is referred to the Web version of this article.)

maximum radii of 1–3 μm generated highest M2/M1 ratio (see Fig. S8 for polarization vs. descriptor rank order plots). The circularity of the topographical features was a strong contributor to the model, with smaller eccentricities producing the greatest increase in macrophage M2 polarization (Fig. S8c). Topographical descriptors had a greater impact on the M2/M1 human macrophage model than on the hiMSC ALP intensity model (i.e. topography plays a larger role in macrophage polarization than in hiMSC osteoinduction). This is consistent with the phagocytic nature of macrophage cells, which engulf bacterial cells and small particles. These analyses illustrate the potential of the ChemoTopoChip and ML for uncovering complex relationships between topography, chemistry, and cell response that offer opportunities for bespoke cell phenotype control using materials design alone.

The hiMSC ALP intensity Random Forest model produced a relatively low correlation between predicted and observed ALP induction (R^2 = 0.46 ± 0.01, Fig. 6a). Difficulties in modelling stem cell responses in polymeric biomaterials has been noted previously [15], in that case due to a relatively small number of polymers with diverse chemotypes driving desirable cell responses. There were therefore insufficient examples of each chemical feature for the ML models to generate rules from. Topographical descriptors identified as being important in the hiMSC ALP model included the size of the topographical features (Table S4 contains list of feature descriptions), with features ≤ 3.5 μm radius increasing ALP expression. However, this trend was not as strong

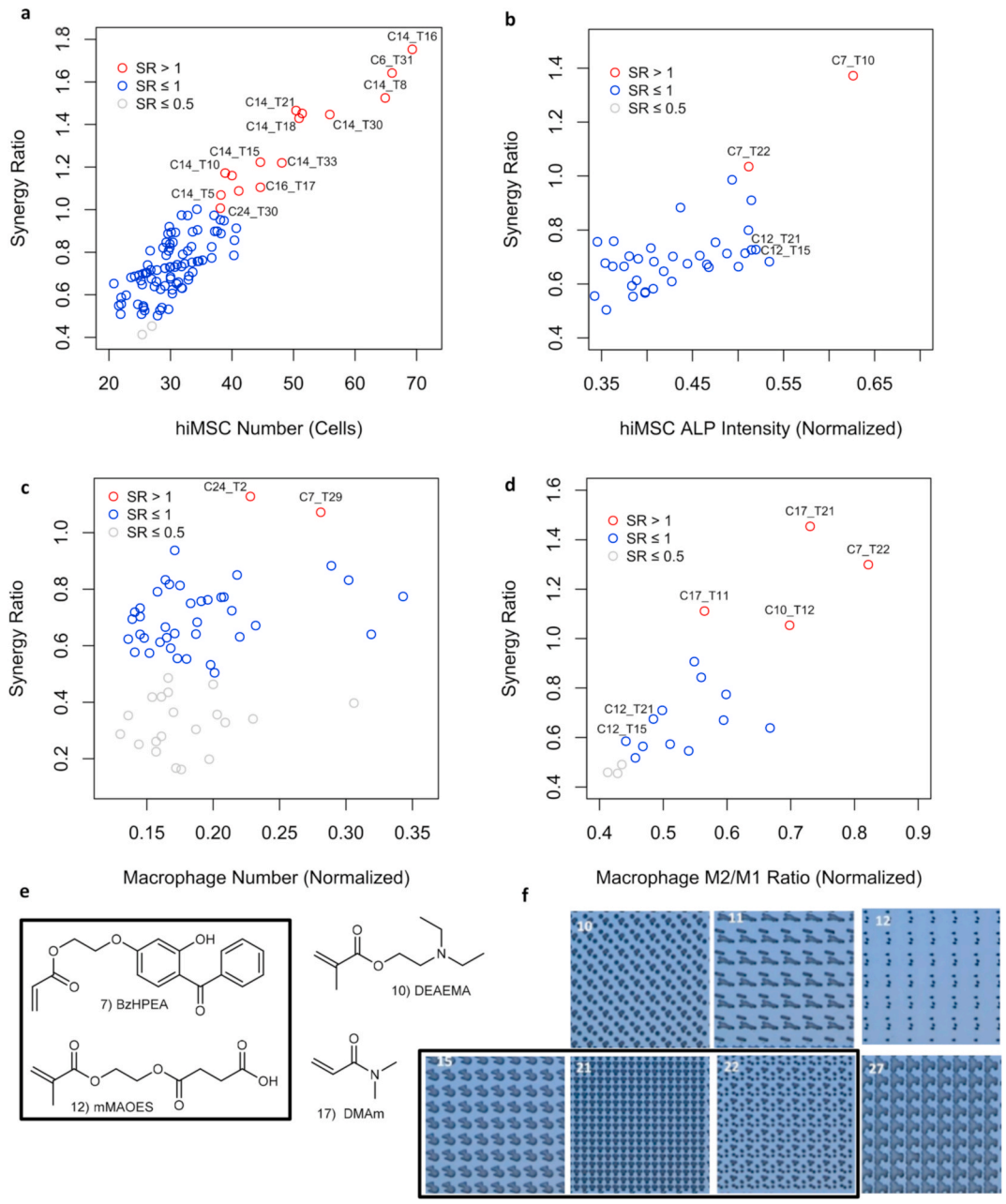

Fig. 5. a) *SR* plotted versus hiMSC cell number; b) *SR* plotted versus hiMSC ALP intensity (normalized); c) *SR* plotted versus human macrophage normalized cell number; d) *SR* plotted versus human macrophage M2/M1 ratio (normalized); e) Selected hit chemistries from macrophage and hiMSC datasets (see Fig. 2 for full list of chemistries). Coincident M2/M1 and ALP hits highlighted in bold; f) Selected hit topographies from macrophage and hiMSC datasets (see Fig. 2 for full list of topographies). Coincident M2/M1 and ALP hits highlighted in the box. See Table S2 and S3 for full analysis of all synergistic combinations.

as that observed for macrophage polarization (see Fig. S9 for ALP upregulation vs. descriptor rank order plots) where cylindrical features of ≤3 μm radius increased M2 polarization. Orientation of topographical features also contributed to the model, with those having a small number (<10%) of features rotated > 25° relative to the x-axis of the Topo unit walls driving an increase in ALP expression.

In polystyrene TopoChip screening of macrophage response, cylindrical pillars with feature size of 5–10 μm radius have also been shown to promote M2 polarization [29]. However, in that work the entire TopoChip selection of 2176 topographies [26] was screened on a polystyrene substrate, in contrast to this study where a selection of 35 topographies (chosen from MSC morphological clustering [36]) were screened in combination with 28 different substrate chemistries. The influence of chemistry, and subset of topographies screened, may account for the small differences in findings between these two studies.

In previous modelling studies of biological responses to polymer libraries, *signature* and other fragment-based molecular descriptors and *Dragon* molecular descriptors have been shown to represent surface chemistries well. These descriptors generated robust, predictive models for diverse biological responses [49]. Paradoxically, in the current study, these types of chemical descriptors were unable to generate ML models for the ChemoTopoChip data that were as accurate as the models using simple 1-hot descriptors to encode the identities of the polymer chemistries. We propose that this is due to the great diversity of the 28 chemistries on the ChemoTopoChip, chosen in order to cover chemical space as widely as possible. The key chemical fragments and resultant descriptors are also therefore very sparse. ML models cannot learn features that are not sufficiently represented in the data set, hence the

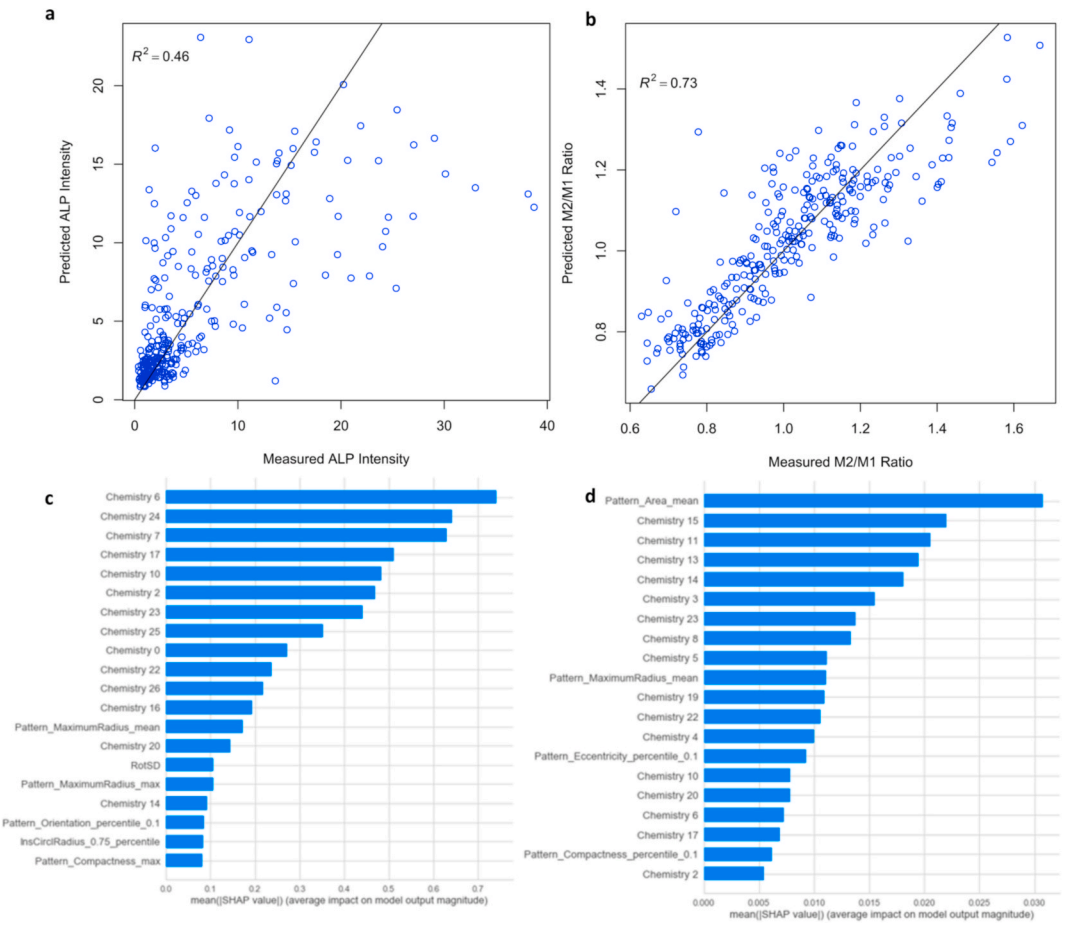

Fig. 6. Scatter plots showing a) hiMSC ALP intensity random forest model using indicator variables for chemistries and topographical descriptors and b) human macrophage polarization random forest model using indicator variables for chemistries and topographical descriptors, line shown is ideal y = x and R^2 corresponds to goodness of fit; c) hiMSC ALP intensity random forest model top contributions; d) human macrophage polarization random forest model top contributions. The plots show the results for a single bootstrap run, not the average of all 50 runs.

combination of high chemical diversity and low number of samples resulted in inadequate information on which to train the ML models, resulting in lower prediction accuracies.

Now the ChemoTopoChip methodology has been established, we anticipate that it can be readily applied to a range of other attachment dependent cell types to determine their propensity to achieve phenotypic modification under substrate instruction. Cell instruction using materials offers many advantages over exogenous soluble factor stimulation (e.g. eliminate off target effects) particularly in the context of medical devices where device surface could be imprinted with bio-instructive cues. In comparison to low throughput cell-material investigations, the ChemoTopoChip experiment requires automated microscopy acquisition and processing capabilities along with topographic molding capability.

4. Conclusions

We have developed the novel ChemoTopoChip platform to screen the potential of both chemistry and topography in producing immunomodulatory materials suitable for bone regenerative applications. Analysis of the hiMSC and human macrophage datasets has identified a range of novel chemistry-topography combinations that surpass the material-instructive cues provided by either alone, with 2-(4-benzoyl-3-hydroxyphenoxy) ethyl acrylate in combination with Topo 22 being synergistic for both cell types. Attachment of both cell types and the hiMSC alkaline phosphatase (ALP) upregulation spanned similar ranges for the large range of chemistries and microtopographies studied, but macrophage polarization was more strongly influenced by chemistry than topography. This large survey of this parameter space allows us to conclude that both chemical and topographical features are important drivers when designing biomaterials for simultaneous control of multiple cell types and act synergistically in some cases. Modelling of the human macrophage polarization data showed that small, cylindrical pillars of <3 μm radius directed macrophage polarization towards an anti-inflammatory phenotype. The size and relative orientation of topographical features was also important for hiMSC ALP expression, with features of ≤ 3.5 μm radius and rotation of $>25^\circ$ relative to the x-axis of the Topo units providing strongest upregulation of ALP. Data generated by the ChemoTopoChip has been shown to be very amenable to machine learning methods, facilitating the development of structure-activity relationships. The methodology illustrated here is equally applicable to other adhesion dependent cells to aid in the design of cell-instructive materials.

Author contributions

This manuscript was written with contributions from all authors. LB manufactured and characterized ChemoTopoChips, carried out image analysis and statistical analysis of results. MHA carried out hiMSC experiments and imaging, MV and BM carried out macrophage experiments and imaging. BK, PM, AS and SV developed the initial ChemoTopoChip platform. GPF and DW performed modelling of data. ILD provided assistance with statistical analysis. AMG, FRAJR, JdB and MRA oversaw project from design to implementation.

Disclosure of potential financial conflicts

Jan de Boer is a founder and shareholder of Materiomics b.v.

Data availability

Raw cell data files, CellProfiler pipelines and topographical descriptors are available in the University of Nottingham Data Repository at http://doi.org/10.17639/nott.7080. Experimental procedures are detailed in the Materials and Methods section; supplementary figures and processed data tables are available in the Supplementary Data section.

Declaration of competing interest

The authors declare the following financial interests/personal relationships which may be considered as potential competing interests: Jan de Boer is a founder and shareholder of Materiomics b.v.

Acknowledgments

This research is supported by funding from the UK's Engineering Physical Sciences Research Council (EPSRC) under the Programme Grant Next Generation Biomaterials Discovery EP/N006615/1. AV and JdB are funded by the European Union's Seventh Framework Programme (FP7/2007-2013) under grant agreement no 289720. AV acknowledge the financial contribution of the Province of Limburg. SV acknowledges the financial support of the European Union's Horizon 2020 Programme (H2020-MSCA- ITN-2015; Grant agreement 676338).

The authors would like to thank Dr Chris Gell (School of Life Sciences Imaging and Microscopy (SLIM) Facility) for assistance with high throughput microscopy.

Appendix A. Supplementary data

Supplementary data to this article can be found online at https://doi.org/10.1016/j.biomaterials.2021.120740.

References

[1] S. Harada, G.A. Rodan, Control of osteoblast function and regulation of bone mass, Nature 423 (2003) 349–355.
[2] A.S. Greenwald, S.D. Boden, V.M. Goldberg, Y. Khan, C.T. Laurencin, R.N. Rosier, Bone-graft substitutes: facts, fictions, and applications, J. Bone Joint Surg. Am. 83 (2001) 98–103.
[3] A. Moshiri, A. Oryan, M. Shahrezaee, An overview on bone tissue engineering and regenerative medicine: current challenges, future directions and strategies, J. Sports Med. Doping Stud. 5 (2015) 1000e144.
[4] S. Samavedi, A.R. Whittington, A.R. Goldstein, Calcium phosphate ceramics in bone tissue engineering: a review of properties and their influence on cell behavior, Acta Biomater. 9 (2013) 8037–8045.
[5] M.J. Dalby, N. Gadegaard, R. Tare, A. Andar, M.O. Riehle, P. Herzyk, C. D. Wilkinson, R.O. Oreffo, The control of human mesenchymal cell differentiation using nanoscale symmetry and disorder, Nat. Mater. 6 (2007) 997–1003.
[6] E. Ngandu Mpoyi, M. Cantini, P.M. Reynolds, N. Gadegaard, M.J. Dalby, M. Salmerón-Sánchez, Protein adsorption as a key mediator in the nanotopographical control of cell behavior, ACS Nano 10 (2016) 6638–6647.
[7] E. Dawson, G. Mapili, K. Erickson, S. Taqvi, K. Roy, Biomaterials for stem cell differentiation, Adv. Drug Deliv. Rev. 60 (2008) 215–228.
[8] D.A. Wang, C.G. Williams, F. Yang, N. Cher, H. Lee, J.H. Elissee, Bioresponsive phosphoester hydrogels for bone tissue engineering, Tissue Eng. 11 (2005) 201–213.
[9] C.R. Nuttelman, M.C. Tripodi, K.S. Anseth, Synthetic hydrogel niches that promote hMSC viability, Matrix Biol. 24 (2005) 208–218.
[10] L. Gong, Y. Zhao, Y. Zhang, Z. Ruan, The macrophage polarization regulates MSC osteoblast differentiation in vitro, Ann. Clin. Lab. Sci. 46 (2016) 65–71.
[11] F. Loi, L.A. Córdova, J. Pajarinen, T. Lin, Z. Yao, S.B. Goodman, Inflammation, fracture and bone repair, Bone 86 (2016) 119–130.
[12] R. Sridharan, A.R. Cameron, D.J. Kelly, C.J. Kearney, F.J. O'Brien, Biomaterial based modulation of macrophage polarization: a review and suggested design principles, Mater. Today 18 (2015) 313–325.
[13] E. Mariani, G. Lisignoli, R.M. Borzi, L. Pulsatelli, Biomaterials: foreign bodies or tuners for the immune response? Int. J. Mol. Sci. 20 (2019) 636.
[14] J. Kohn, New approaches to biomaterials design, Nat. Mater. 3 (2004) 745–747.
[15] A.D. Celiz, J.G.W. Smith, A.K. Patel, A.L. Hook, D. Rajamohan, V.T. George, M. J. Patel, V.C. Epa, T. Singh, R. Langer, D.G. Anderson, N.D. Allen, D.C. Hay, D. A. Winkler, D.A. Barrett, M.C. Davies, L.E. Young, C. Denning, M.R. Alexander, Discovery of a novel polymer for human pluripotent stem cell expansion and multilineage differentiation, Adv. Mater. 27 (2015) 4006–4012.
[16] R. Zhang, H.K. Mjoseng, M.A. Hoeve, N.G. Bauer, S. Pells, R. Besseling, S. Velugotla, G. Tourniaire, R.E.B. Kishen, Y. Tsenkina, C. Armit, C.R.E. Duffy, M. Helfen, F. Edenhofer, P.A. de Sousa, M. Bradley, A thermoresponsive and chemically defined hydrogel for long-term culture of human embryonic stem cells, Nat. Commun. 4 (2013) 1335.
[17] A.K. Patel, A.D. Celiz, D. Rajamohan, D.G. Anderson, R. Langer, M.C. Davies, M. R. Alexander, C. Denning, A defined synthetic substrate for serum-free culture of human stem cell derived cardiomyocytes with improved functional maturity identified using combinatorial materials discovery, Biomaterials 61 (2015) 257–265.
[18] D.C. Hay, S. Pernaglio, J.J. Diaz-Mochon, C.N. Medine, S. Greenhough, Z. Hannoun, J. Schrader, J.R. Black, J. Fletcher, D. Dalgetty, A.I. Thompson, P. N. Newsome, S.J. Forbes, J.A. Ross, M. Bradley, J.P. Iredale, Unbiased screening of polymer libraries to define novel substrates for functional hepatocytes with inducible drug metabolism, Stem Cell Res. 6 (2011) 92–102.
[19] H.M. Rostam, L.E. Fisher, A.L. Hook, L. Burroughs, J.C. Luckett, G.P. Figueredo, C. Mbadugha, A.C.K. Teo, A. Latif, L. Kämmerling, M. Day, K. Lawler, D. Barrett, S. Elsheikh, M. Ilyas, D.A. Winkler, M.R. Alexander, A.M. Ghaemmaghami, Immune-instructive polymers control macrophage phenotype and modulate the foreign body response in vivo, Matter 2 (2020) 1564–1581.
[20] A.L. Hook, C.Y. Chang, J. Yang, J. Luckett, A. Cockayne, S. Atkinson, Y. Mei, R. Bayston, D.J. Irvine, R. Langer, D.G. Anderson, P. Williams, M.C. Davies, M. R. Alexander, Combinatorial discovery of polymers resistant to bacterial attachment, Nat. Biotechnol. 30 (2012) 868–875.
[21] N. Jeffery, K. Kalenderski, J. Dubern, A. Lomiteng, M. Dragova, A. Frost, B. Macrae, A. Mundy, M. Alexander, P. Williams, D. Andrich, A new bacterial resistant polymer catheter coating to reduce catheter associated urinary tract infection (CAUTI): a first-in-man pilot study, Eur. Urol. Suppl. 18 (2019) e377.
[22] A. Curtis, C. Wilkinson, Topographical control of cells, Biomaterials 18 (1997) 1573–1583.
[23] Y.Y. Amin, K. Runager, F. Simoes, A. Celiz, Taresco V. RosR, J.J. Enghild, L. A. Abildtrup, D.C. Kraft, D.S. Sutherland, M.R. Alexander, M. Foss, R. Ogaki, Combinatorial biomolecular nanopatterning for high-throughput screening of stem-cell behavior, Adv. Mater. 28 (2016) 1472–1476.
[24] P. Roach, T. Parker, N. Gadegaard, M.R. Alexander, A bio-inspired neural environment to control neurons comprising radial glia, substrate chemistry and topography, Biomater. Sci. 1 (2013) 83–93.
[25] J. Yang, F.R.A.J. Rose, N. Gadegaard, M.R. Alexander, A high-throughput assay of cell-surface interactions using topographical and chemical gradients, Adv. Mater. 21 (2009) 300–304.
[26] H.V. Unadkat, M. Hulsman, K. Cornelissen, B.J. Papenburg, R.K. Truckenmüller, A. E. Carpenter, M. Wessling, G.F. Post, M. Uetz, M.J.T. Reinders, D. Stamatialis, C. A. van Blitterswijk, J. de Boer, An algorithm-based topographical biomaterials library to instruct cell fate, Proc. Natl. Acad. Sci. U.S.A. 108 (2011) 16565–16570.
[27] F.F.B. Hulshof, B. Papenburg, A. Vasilevich, M. Hulsman, Y. Zhao, M. Levers, N. Fekete, M. de Boer, H. Yuan, S. Shantanu, N. Beijer, M.A. Bray, D.J. Logan, M. Reinders, A.E. Carpenter, C. van Blitterswijk, D. Stamatialis, J. de Boer, Mining for osteogenic surface topographies: in silico design to in vivo osseo-integration, Biomaterials 137 (2017) 49–60.
[28] A.S. Vasilevich, F. Mourcin, A. Mentink, F. Hulshof, N. Beijer, Y. Zhao, M. Levers, B. Papenburg, S. Singh, A.E. Carpenter, D. Stamatialis, C. van Blitterswijk, K. Tarte, J. de Boer, Designed surface topographies control ICAM-1 expression in tonsil-derived human stromal cells, Front. Bioeng. Biotechnol. 6 (2018) 87.
[29] M.J. Vassey, G.P. Figueredo, D.J. Scurr, A.S. Vasilevich, S. Vermeulen, A. Carlier, J. Luckett, N.R.M. Beijer, P. Williams, D.A. Winkler, J. de Boer, A. M. Ghaemmaghami, M.R. Alexander, Immune modulation by design: using topography to control human monocyte attachment and macrophage differentiation, Adv. Sci. 7 (2020) 1903392.
[30] Y.K.R. Chandorkar, B. Basu, The foreign body response demystified, ACS Biomater. Sci. Eng. 5 (2019) 19–44.
[31] A.J. Vegas, O. Veiseh, M. Gürtler, J.R. Millman, F.W. Pagliuca, A.R. Bader, J. C. Doloff, J. Li, M. Chen, K. Olejnik, H.H. Tam, S. Jhunjhunwala, E. Langan, S. Aresta-Dasilva, S. Gandham, J.J. McGarrigle, M.A. Bochenek, J. Hollister-Lock, J. Oberholzer, D.L. Greiner, G.C. Weir, D.A. Melton, R. Langer, D.G. Anderson, Long-term glycemic control using polymer-encapsulated human stem cell–derived beta cells in immune-competent mice, Nat. Med. 22 (2016) 306–311.
[32] J.C. Doloff, O. Veiseh, A.J. Vegas, H.H. Tam, S. Farah, M. Ma, J. Li, A. Bader, A. Chiu, A. Sadraei, S. Aresta-Dasilva, M. Griffin, S. Jhunjhunwala, M. Webber, S. Siebert, K. Tang, M. Chen, E. Langan, N. Dholokia, R. Thakrar, M. Qi, J. Oberholzer, D.L. Greiner, R. Langer, Daniel G. Anderson, Colony stimulating factor-1 receptor is a central component of the foreign body response to biomaterial implants in rodents and non-human primates, Nat. Mater. 16 (2017) 671–680.
[33] A.D. Celiz, J.G.W. Smith, R. Langer, D.G. Anderson, D.A. Winkler, D.A. Barrett, M. C. Davies, L.E. Young, C. Denning, M.R. Alexander, Materials for stem cell factories of the future, Nat. Mater. 13 (2014) 570–579.
[34] D. Li, Q. Zheng, Y. Wang, H. Chen, Combining surface topography with polymer chemistry: exploring new interfacial biological phenomena, Polym. Chem. 5 (2014) 14–24.

[35] Q. Li, B. Zhang, N. Kasoju, J. Ma, A. Yang, Z. Cui, H. Wang, H. Ye, Differential and interactive effects of substrate topography and chemistry on human mesenchymal stem cell gene expression, Int. J. Mol. Sci. 19 (2018) 2344.
[36] A. Vasilevich, S. Vermeulen, M. Kamphuis, N. Roumans, S. Eroume, D.G.A. J. Hebels, R. Reihs, N. Beijer, A. Carlier, A.E. Carpenter, S. Singh, J. de Boer, bioRxiv preprint. https://doi.org/10.1101/2020.05.13.093641, 2020.
[37] S.I. Miller, Dissociation energies of π-bonds in alkenes, J. Chem. Educ. 55 (1978) 778–780.
[38] B. de B. Darwent, Bond dissociation energies in simple molecules. National standard reference data series, National Bureau of Standards 31 (1970). Washington.
[39] S. Ray, A.G. Shard, Quantitative analysis of adsorbed spectroscopy, Anal. Chem. 83 (2011) 8659–8666.
[40] L. Balducci, BlaA, M. Saldarelli, A. Soleti, A. Pessina, A. Bonomi, V. Coccè, M. Dossena, V. Tosetti, V. Ceserani, S.E. Navone, M.L. Falchetti, E.A. Parati, G. Alessandri, Immortalization of human adipose-derived stromal cells: production of cell lines with high growth rate, mesenchymal marker expression and capability to secrete high levels of angiogenic factors, Stem Cell Res. Ther. 5 (2014) 63.
[41] T. Mori, T. Kiyono, H. Imabayashi, Y. Takeda, K. Tsuchiya, S. Miyoshi, H. Makino, K. Matsumoto, H. Saito, S. Ogawa, M. Sakamoto, J. Hata, A. Umezawa, Combination of hTERT and bmi-1, E6, or E7 induces prolongation of the life span of bone marrow stromal cells from an elderly donor without affecting their neurogenic potential, Mol. Cell Biol. 25 (2005) 5183–5195.
[42] F. Salazar, L. Hall, O.H. Negm, D. Awuah, P.J. Tighe, F. Shakib, A. M. Ghaemmaghami, The mannose receptor negatively modulates the Toll-like receptor 4–aryl hydrocarbon receptor–indoleamine 2,3-dioxygenase axis in dendritic cells affecting T helper cell polarization, J. Allergy Clin. Immunol. 137 (2016) 1841–1851.
[43] A.E. Carpenter, T.R. Jones, M.R. Lamprecht, C. Clarke, I.H. Kang, O. Friman, D. A. Guertin, J.H. Chang, R.A. Lindquist, J. Moffat, P. Golland, D.M. Sabatini, CellProfiler: image analysis software for identifying and quantifying cell phenotypes, Genome Biol. 7 (2006) R100.
[44] Y. Benjamini, Y. Hochberg, Controlling the false discovery rate: a practical and powerful approach to multiple testing, J. R. Stat. Soc. Series B 57 (1995) 289–300.
[45] B.S. Everitt, S. Landau, M. Leese, Cluster Analysis, fourth ed., 2001.
[46] D.P. Nair, N.B. Cramer, T.F. Scott, C.N. Bowman, R. Shandas, Photopolymerized thiol-ene systems as shape memory polymers, Polymer 51 (2010) 4383–4389.
[47] A. Rutkovskiy, K.O. Stensløkken, I.J. Vaage, Osteoblast differentiation at a glance, Med. Sci. Monit. Basic Res. 22 (2016) 95–106.
[48] L. Breiman, Random forests, Mach. Learn. 45 (2001) 5–32.
[49] P. Mikulskis, M.R. Alexander, D.A. Winkler, Toward interpretable machine learning models for materials discovery, Adv. Intel. Syst. 1 (2019) 190045.